Click Here for Full Article

Seismic tomography of Taiwan: Improved constraints from a dense network of strong motion stations

Yih-Min Wu,[1] Chien-Hsin Chang,[2] Li Zhao,[3] J. Bruce H. Shyu,[4] Yue-Gau Chen,[1] Kerry Sieh,[4] and Jean-Philippe Avouac[4]

[1]   In this study, a large collection of 41,141 S-P times from the untapped records of the Taiwan Strong Motion Instrumentation Program (TSMIP) network is combined with the P and S wave arrival times from the Taiwan Central Weather Bureau Seismic Network (CWBSN) to image the V_p and V_p/V_s structures beneath Taiwan. The records from the 680 TSMIP stations throughout Taiwan in the past 15 years enhance the path coverage and the resolution in the tomography inversions tremendously. Our result for the V_p structure largely confirms previous studies but brings better constraint on the V_p/V_s structure. The colliding Luzon volcanic arc is characterized by a belt of high V_p and high V_p/V_s with high seismicity that includes the offshore islands of Lutao and Lanyu and the Coastal Ranges in eastern Taiwan, at the depth between about 13 and 25 km. This high V_p/V_s belt can be traced to the subduction zone in the region between Hualian and Ilan in the deeper portion. The shallow portions of the southwestern coastal plain and the Pingtung region are also characterized by a belt of high V_p/V_s with lower seismicity. Most of the events occurred at the base of the high V_p/V_s zones. We suggest that material strength in those regions may be too low to accumulate stress, which may indicate water-saturated young sediments. Finally, the Central Range region is characterized by a low V_p/V_s belt.

Citation: Wu, Y.-M., C.-H. Chang, L. Zhao, J. B. H. Shyu, Y.-G. Chen, K. Sieh, and J.-P. Avouac (2007), Seismic tomography of Taiwan: Improved constraints from a dense network of strong motion stations, *J. Geophys. Res.*, *112*, B08312, doi:10.1029/2007JB004983.

1. Introduction

[2]   Taiwan is situated in the western portion of the Pacific Rim seismic belt. In the east, the Philippine Sea plate subducts northward under the Eurasian plate along the Ryukyu trench. Off the southern tip of Taiwan, the South China Sea subplate, part of the Eurasian plate, subducts eastward under the Philippine Sea plate. Figure 1 is a schematic diagram showing the major geologic settings in the region. Most of Taiwan is under a northwest-southeast (NW-SE) compression with a convergence rate of about 8 cm/yr [*Yu et al.*, 1997]. The Taiwan orogeny, started around 4 Ma [*Suppe*, 1984], is relatively young on the geological timescale. The island has a high rate of crustal deformation and a strong seismic activity, and many disastrous earthquakes have occurred in the past. These damaging earthquakes can be divided into two general classes: earthquakes offshore Hualien due to the subduction of the

Philippine Sea plate northward under the Eurasian plate, and the ones associated with active faults on the main island.

[3]   The Longitudinal Valley in the southeast (4 in Figure 1) is the suture zone of Eurasian and Philippine Sea plates, and separates Taiwan into two major tectonic provinces. The eastern side consists of the Coastal Ranges and several volcanic islands, and is the leading edge of the Philippine Sea plate. The western province is associated with the Eurasian continental shelf [*Ho*, 1999] and can be classified into four NNE-SSW trending geological belts. They are, from west to east, the Coastal Plain, the Western Foothills, the Hsueshan Ranges, and the Central Ranges.

[4]   One of the earlier tomographic studies in the Taiwan region was carried out by *Roecker et al.* [1987] using the P wave arrival times observed by the Taiwan Telemetered Seismographic Network (TTSN). The TTSN was operated by the Institute of Earth Sciences, Academia Sinica, and consisted of only 25 stations equipped with vertical component, short-period seismometers. The network provided very limited coverage on the three-dimensional (3-D) seismic structure in the region.

[5]   The TTSN was incorporated into the Central Weather Bureau Seismic Network (CWBSN) in 1991. Since then, many more stations have been added to the CWBSN, which now consists of 71 telemetered stations equipped with three-component S13 seismometers. Figure 2 shows the station distribution of the CWBSN. *Rau and Wu* [1995]

---

[1]Department of Geosciences, National Taiwan University, Taipei, Taiwan.
[2]Central Weather Bureau, Taipei, Taiwan.
[3]Institute of Earth Sciences, Academia Sinica, Nankang, Taipei, Taiwan.
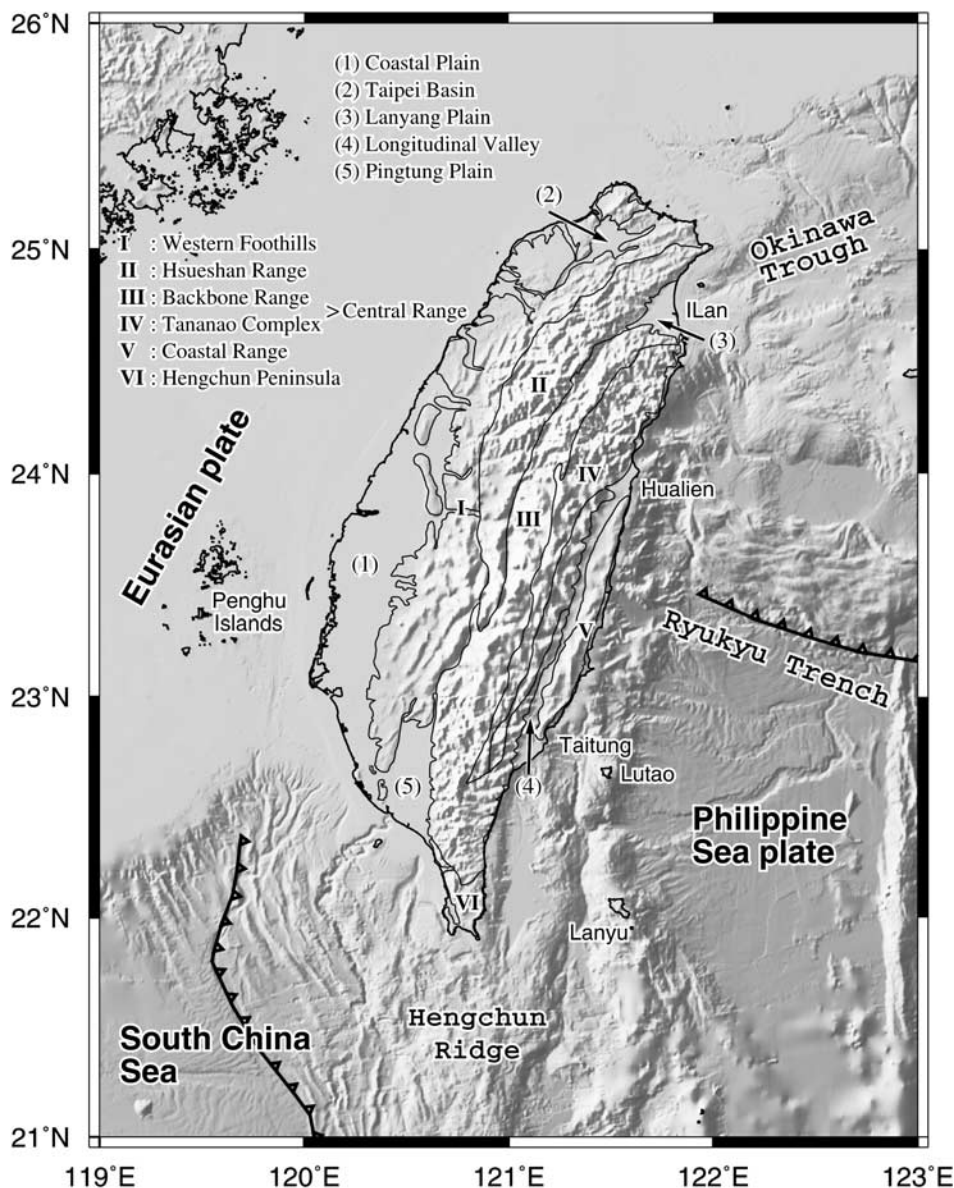[4]Tectonics Observatory, California Institute of Technology, Pasadena, California, USA.

Figure 1. Topography and geological settings of the Taiwan region.

used the *P* wave arrival times from the CWBSN to invert for a 3-D *P* wave velocity structure. Using both *P* and *S* wave arrival times from the CWBSN, *Ma et al.* [1996] and *Shin and Chen* [1988] determined the *P* and *S* wave velocity models. More recently, *Kim et al.* [2005] conducted a tomography study for 3-D *P* and *S* wave velocity structures by jointly using data sets from the CWBSN and two temporary seismic arrays in Hualien and Pingtung [*Chen*, 1995, 1998]. In a more recent study by *Wang et al.* [2006], arrival times from both local and teleseismic events were used to achieve a good resolution at greater depths.

[6] There is yet another huge untapped reservoir of seismic records. In 1991, Taiwan's Central Weather Bureau undertook a major effort to establish the TSMIP, which has 680 digital accelerographs in free field sites [*Shin et al.*, 2003]. Apart from the unpopulated high mountain areas, the TSMIP stations have achieved an average station spacing of a few kilometers. Figure 2 also shows the station distribu-

tion of the TSMIP network. During the past 15 years, a large number of high-quality digital accelerograms have been recorded from tens of thousands of earthquakes of magnitudes M = 2 to M = 7. These waveform records, combined with the seismograms recorded by the CWBSN, provide an excellent database for seismological studies.

[7] Previous 3-D *P* and *S* wave velocity structure inversions [e.g., *Rau and Wu*, 1995; *Ma et al.*, 1996; *Shin and Chen*, 1988; *Kim et al.*, 2005] have only used the CWBSN stations and therefore have not taken advantage of the vast amount of information provided by the TSMIP stations. We have conducted the very first tomographic study using the 15 years worth of information contained in the TSMIP seismograms. An almost tenfold increase in station distribution provided by the 680 TSMIP stations over the CWBSN network enables us to achieve unprecedented high-resolution and reliable images of the 3-D seismic structure beneath Taiwan. Even though most of the earlier
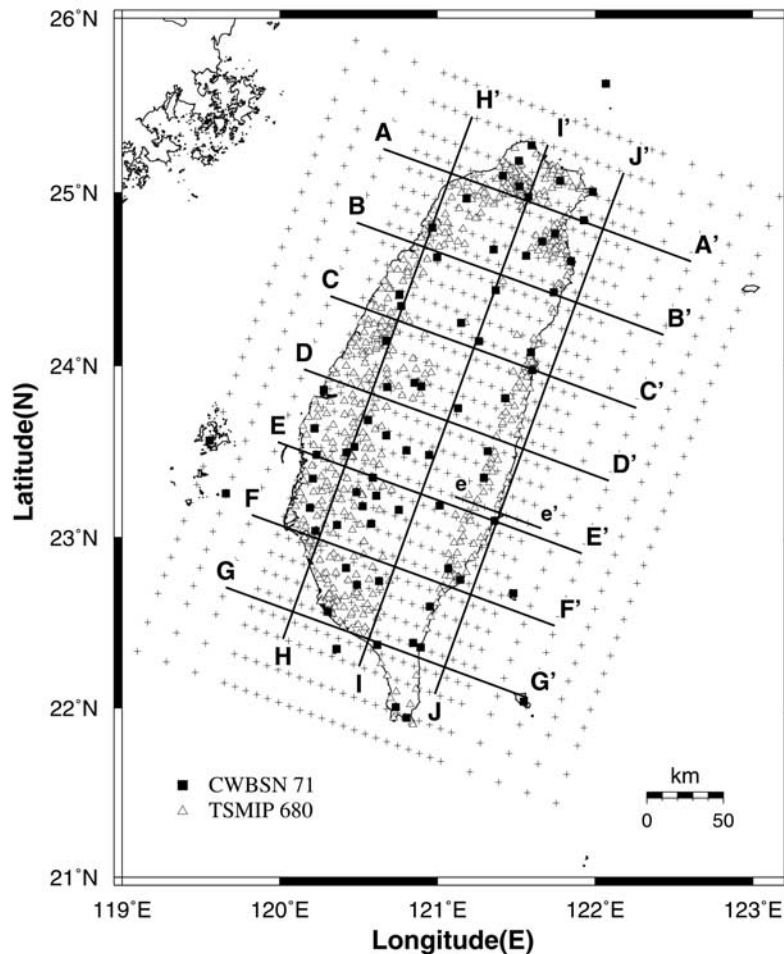
Figure 2. Station distributions of the CWBSN and TSMIP. Also shown are the grid setting used in this study for tomography inversions and the locations for A-A′ to J-J′ profiles in Figure 6 and the e-e′ profile in Figure 8.

TSMIP stations were not equipped with absolute timing systems, the S-P times can still be effectively used to obtain the 3-D V_p/V_s model and to improve the earthquake locations.

2. Data and Method

[8] The hypocentral distribution of the events used in this study is shown in Figure 3. The selection of the earthquakes was based on the following criteria: (1) earthquakes occurred in the period from 1 January 1992 to 31 December 2005 and inside the box shown in Figure 3; (2) in each $0.1° \times 0.1° \times 10$ km cubic cell, we selected three events recorded by the largest number of CWBSN stations; (3) events for which the TSMIP network offered at least one good quality reading of S-P time. In the end a total of 299,104 P wave arrival times and 133,062 S-P times from the CWBSN, and 41,141 S-P times from the TSMIP were obtained from 17,206 regional earthquakes. The P and S wave arrival times at the CWBSN stations are available from the Central Weather Bureau (CWB) catalog. We used the S wave arrival times in the inversions only in the form of S-P times. The S-P times from the TSMIP network were picked manually from the strong motion waveforms. Large earthquakes may

be recorded by many strong motion stations. Small events can only be recorded by stations very close to the epicenters because of the triggering threshold of the strong motion seismometers. Thus the S-P times for most events were obtained from a few stations. However, the dense distribution of the 680 strong motion stations provides a great enhancement in path coverage in the tomography inversions. The P and S arrivals from the CWBSN were also repicked and only data with weightings 0, 1, 2 and 3 were used in this study. The arrivals weighting is the standard scheme used in HYPO71 [Lee and Lahr, 1975].

[9] The velocity model is specified on a set of 3-D spatial grid points, and a linear interpolation is adopted between the grid points. Figure 2 also shows the distribution of the 28 × 32 grid points on a horizontal plane. In depth, a total of 17 grid points are distributed at depths of 0, 2, 4, 6, 9, 13, 17, 21, 25, 30, 35, 50, 70, 90, 110, 140, and 200 km. The grid spacings in NWW-SEE and NNE-SWW directions are 7.5 km and 12.5 km for most of the Taiwan region, respectively. The grid spacing for offshore region is 20 km. The given of different grid spacing is considering the stations coverage and geological settings of Taiwan.
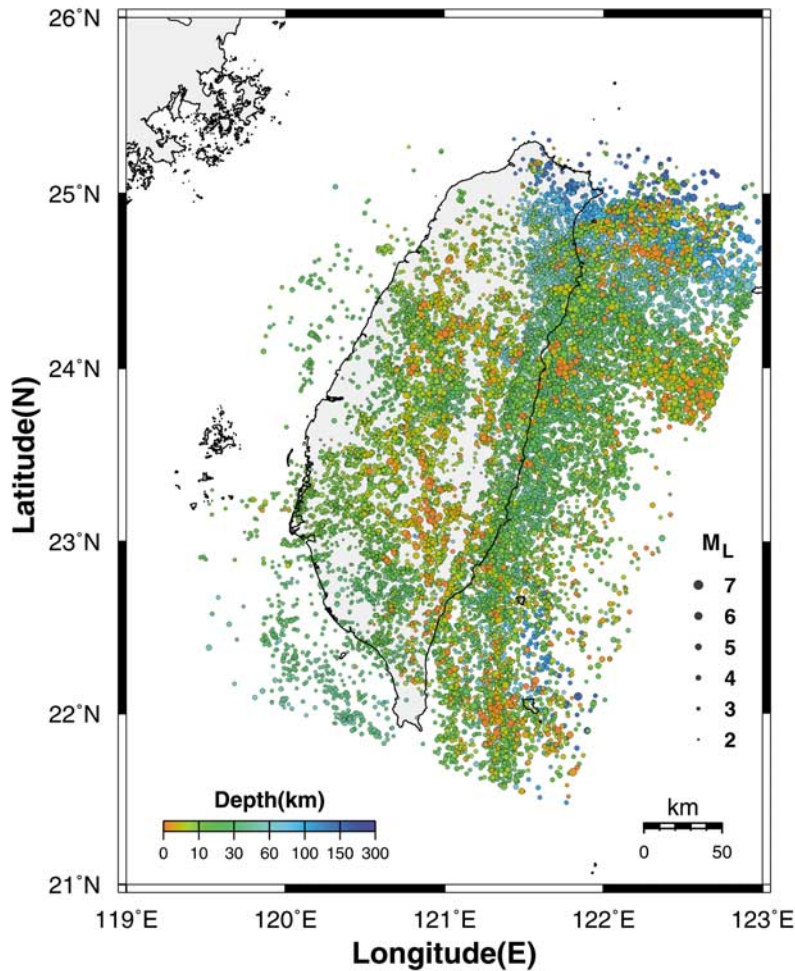
Figure 3. Hypocenter distribution of the 17,206 events used in this study.

[10] We applied the algorithms SIMULPS12 [*Evans et al.*, 1994] based on the inversion method by *Thurber* [1983, 1993], *Eberhart-Phillips* [1990], and *Thurber and Eberhart-Phillips* [1999]. Ray tracing is accomplished using an approximate 3-D algorithm with curved nonplanar raypaths [*Um and Thurber*, 1987]. We used the damped least squares inversion based on the parameter separation techniques of *Pavlis and Booker* [1980].

[11] The damping values of 35 for V_p and 40 for V_p/V_s were chosen empirically by running a series of single-iteration inversions with a range of damping values, and finding the tradeoff between data misfits and the model variances [*Eberhart-Phillips*, 1986, 1993]. The units for the V_p and V_p/V_s dampings are s^2 and unitless [*Evans et al.*, 1994], respectively. A consistent damping was used in the entire iterative inversion process. Each iteration consists of two steps: event relocation and then structural inversion. In order to achieve numerical stability, we have imposed the maximum velocity perturbations of 0.5 km/s for V_p and 0.25 for V_p/V_s. The velocity structural inversion reached convergence after three iterations.

[12] The initial 3-D velocity models were constructed based on a one-dimensional (1-D) horizontally layered

P wave velocity model and a reference V_p/V_s ratio determined using the VELEST program [*Kissling et al.*, 1994]. The initial models (Table 1) generally agree with the 1-D horizontally layered P and S wave velocity models that

Table 1. Initial Models of V_p and V_p/V_s Ratio Used in This Study

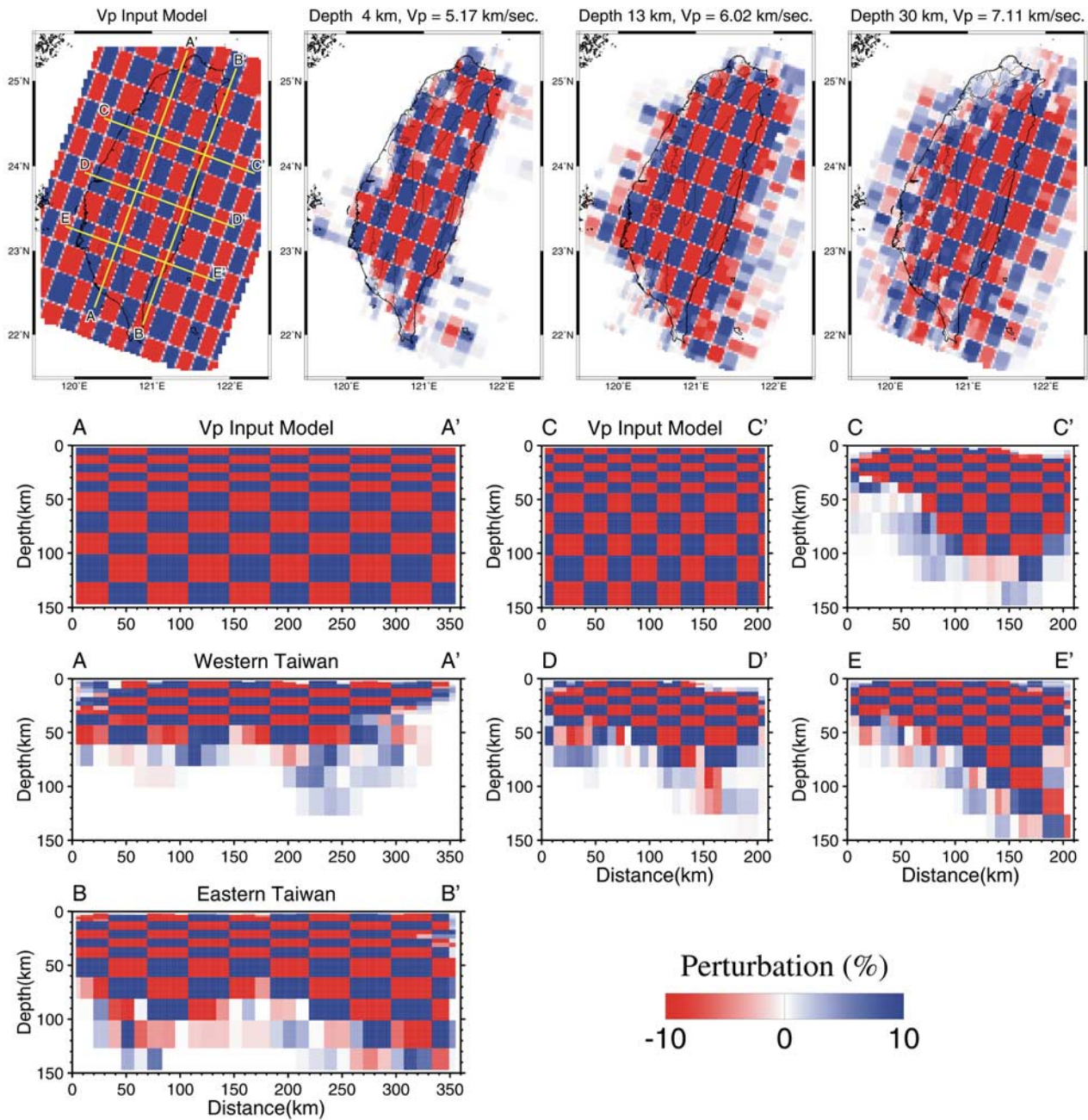| Depth, km	V_p, km/s	V_p/V_s Ratio
0	3.90	1.87
2	4.64	1.76
4	5.17	1.72
6	5.22	1.71
9	5.64	1.71
13	6.02	1.73
17	6.30	1.74
21	6.58	1.74
25	6.74	1.74
30	7.11	1.74
35	7.52	1.74
50	7.98	1.73
70	8.25	1.75
90	8.28	1.72
110	8.38	1.73
140	8.40	1.74
200	8.70	1.74
700	9.00	1.73

Figure 4a. Input and recovered models in V_p checkerboard resolution test. Input model is shown in (top left) map view and two profiles A-A′ and C-C′ (second row). All the other panels are recovered model. (top) Map views are plotted at three depths, and profiles are provided for A-A′ to E-E′ whose locations are indicated in the top left.

were proposed by *Shin and Chen* [1988] and used currently by the CWB for routine event locations.

3. Resolution Test

[13] We used the checkerboard resolution test (CRT) and the restoring resolution test (RRT) proposed by *Zhao et al.* [1992] and *Hole et al.* [2000] to examine how well of the velocity structure on heterogeneities can be retrieved from the inversions. The CRT method can be used to investigate the spatial resolution provided by the existing ray coverage.

We constructed the checkerboard velocity models by adding ±10% of velocity variation to our initial models with about 22.5 × 37.5 × 8 km block (Figures 4a and 4b), leading to 20% velocity discontinuity across the boundary of checkerboard boxes. Synthetic traveltimes were calculated from each selected hypocenter to the recording stations through the checkerboard velocity models. Then the synthetic data were inverted for the velocity perturbations from the initial models. We used the same procedures and parameters in the CRT inversions as those used in the inversions of real data.
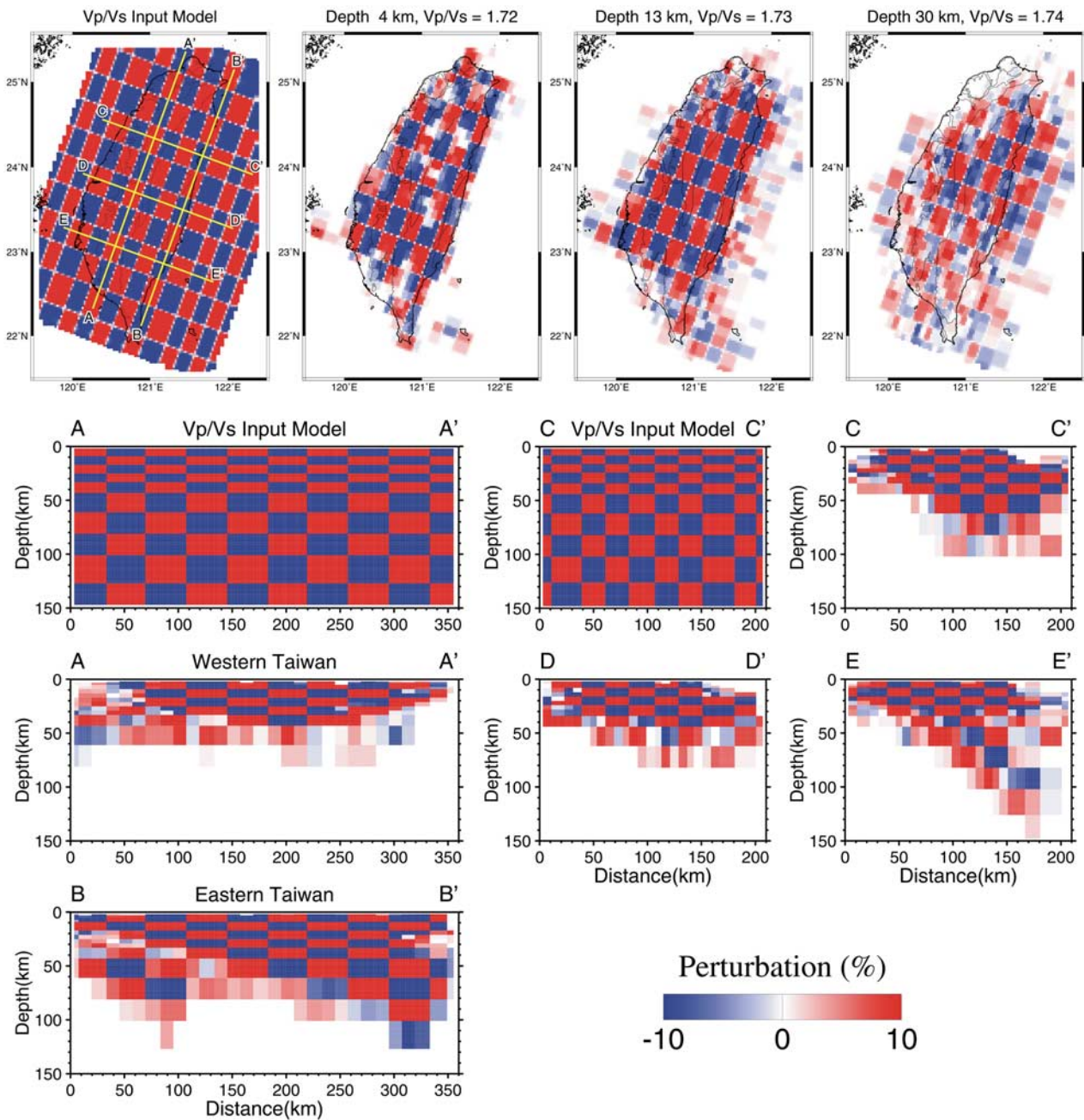
Figure 4b. Input and recovered models in V_p/V_s checkerboard resolution test. Input model is shown in (top left) map view and two profiles A-A′ and C-C′ (second row). All the other panels are recovered model. (top) Map views are plotted at three depths, and profiles are provided for A-A′ to E-E′ whose locations are indicated in the top left.

[14] Figure 4a shows a few horizontal and vertical slices of the CRT input and recovered models for the P wave velocity structures. Since most of the stations are located on land, a good P wave structure recovery underneath Taiwan is achieved. The region of good recovery extends into the eastern offshore region at a greater depth because of occurrence of deeper earthquakes there. In western Taiwan the resolution is excellent at depths down to about 60 km (e.g., profile AA′ in Figure 4a). In contrast, in eastern Taiwan a similar resolution can be achieved at a greater

depth down to about 100 km (e.g., profile BB′ in Figure 4a), and still deeper in the subduction zone regions in northeastern and southeastern Taiwan.

[15] Figure 4b shows several horizontal and vertical slices for the CRT input and recovered models for the V_p/V_s structure. Determining the S wave arrival times is generally more difficult than for the P wave. Therefore the recovery of V_p/V_s structure is not as good as that seen in Figure 4a for the resolution of P wave structure. The CRT results show that a good V_p/V_s resolution can be obtained down to 40-km

depth in western Taiwan and 80-km depth in eastern Taiwan (e.g., profiles AA′ and BB′ in the Figure 4b). However, a better resolution for V_p/V_s structure than for P wave structure can be seen at shallow depth in the westernmost part of the island of Taiwan (e.g., the slice for 4-km depth in Figures 4a and 4b). This is because we used a large number of S-P times from the TSMIP network.

4. Results and Tectonic Interpretations

4.1. V_p and V_p/V_s Structures

[16] Figures 5a and 5b presents the map views at several depths for the results of V_p and V_p/V_s structures determined in this study. The 3-D V_p structure from our inversion largely agree with that obtained in previous studies [e.g., *Roecker et al.*, 1987; *Rau and Wu*, 1995; *Ma et al.*, 1996; *Shin and Chen*, 1998; *Kim et al.*, 2005]. However, the 3-D V_p/V_s structure we derived with the help of enhanced station coverage provided by the TSMIP network provides additional insights into the first-order structures of the Taiwan orogeny. In shallow (<10 km deep) layers, there are V_p and V_p/V_s anomalies that are associated with near-surface geologic units. Most notably are the areas of low V_p and high V_p/V_s that reflect the water-saturated young sediments of the coastal basins in western Taiwan. Smaller areas with similar signals near both the northern and southern ends of the Longitudinal Valley may correspond to large amount of young sediments there. Neogene sedimentary rocks in the Western Foothills are characterized by low V_p and low V_p/V_s. Farther east, high V_p coincides with the high mountain ranges of Taiwan, including the Hsueshan and Central Ranges.

[17] At about 10-km depth, most of the sedimentary basins have bottomed out, with a clear exception of the Pingtung Plain, where low V_p and high V_p/V_s signals are present down to a depth of 17 km. The rapidly subsiding Pingtung Plain is likely to be the surface manifestation of the subducting oceanic lithosphere, just prior to the collision of the fore-arc ridge and the continental margin [e.g., *Shyu et al.*, 2005a], since the northern boundary of the basin is coincident with the northern edge of the Wadati-Benioff zone of the Manila trench [e.g., *Huang et al.*, 1992; *Kao et al.*, 2000]. The large depth of sediments in the basin is also consistent with this hypothesis.

[18] Another interesting feature that is visible at the depth between 9 and 17 km is the high V_p and high V_p/V_s signal extending from the Penghu Islands into the westernmost coastal plain of Taiwan. This feature appears to be consistent with the proposed Peikang Basement High (PKH [e.g., *Mouthereau et al.*, 2002]). However, its signal is also consistent with the presence of mafic rocks, such as the basaltic outcrops in the Penghu Islands.

[19] A very sharp boundary between high and low V_p coincides with the Longitudinal Valley in eastern Taiwan below about 17-km depth. High V_p to the east of this boundary clearly reflects the oceanic crust of the Philippine Sea plate. The Central Ranges west of this boundary, however, has much lower V_p. This indicates clearly that a fundamental material difference exists between the oceanic Philippine Sea plate and the basement of the Central Ranges. The significant difference in V_p across the Longitudinal Valley supports the notion that the valley is a major suture zone. The moderately low V_p/V_s below the Central

Ranges belt is, in fact, consistent with the hypothesized granitic continental rocks that form the basement of the Central Ranges belt. If the Central Ranges belt was formed by accretionary prism, it would have a high V_p/V_s ratio from water saturation. Recently, it has been proposed that the Central Ranges of Taiwan and its southern extension in the Hengchun Peninsula and the submarine Hengchun Ridge may be a continental sliver, and that the Taiwan orogeny is produced by a tandem suturing between the Eurasian continental margin, the Luzon volcanic arc, and this intervening continental sliver [*Shyu et al.*, 2005b]. The fact that virtually no major discontinuity in V_p structure can be seen between the Central Ranges and the Hengchun Peninsula supports the idea that they may belong to a continuous belt.

[20] The colliding Luzon volcanic arc is also characterized by a belt of high V_p/V_s that includes the offshore islands of Lutao and Lanyu, and the Coastal Ranges in eastern Taiwan, at the depth between about 13 and 25 km. This high V_p/V_s belt may indicate fluids in the crust at depth, possibly along the major fault zones of the suture.

4.2. V_p and V_p/V_s Profiles

[21] Profiles of V_p and V_p/V_s, augmented by relocated seismicity, provide further constraints on the crustal structures across the Taiwan orogeny. Figures 6a and 6b present some of the profiles with the locations of the profiles depicted in Figure 2. Also indicated in Figures 6a and 6b is the topography of a reference Moho boundary corresponding to $V_p = 7.8$ km/s (thin white line in the V_p profiles). The Moho appears to be the deepest below the central to eastern Central Ranges, down to about 60-km depth, in agreement with previous estimates by *Yeh et al.* [1998] and *Kim et al.* [2005]. This indicates that significant crustal thickening has occurred in the Central Ranges belt. In the northernmost profile (A-A′), the crustal thickness is much smaller. Profiles E-E′, F-F′, and J-J′ show relatively deep boundary of $V_p = 7.8$ km/s in the eastern Taiwan and offshore region, beneath the Luzon volcanic arc. The volcanic activity may be involved. Because of possible involvement of the volcanic activity in this region, the Moho interface there may be more complex.

[22] In most of the profiles, western Taiwan is characterized by a thick wedge of either sedimentary rocks or young sediments of low V_p. Thick piles of young sediments are more prominent as high V_p/V_s wedges in southwestern Taiwan between profiles D-D′ and F-F′. This young sediment wedge appears to hamper the occurrence of background seismicity. This is clearly illustrated in the longitudinal profile H-H′, in which almost no earthquake of M > 3.0 occurred in the high V_p/V_s wedge. However, many earthquakes occur at the base of this wedge. This indicates that many of the active structures in southwestern Taiwan have extended farther into the coastal plain as blind faults beneath the young coastal plain sediments.

[23] Few earthquakes and a low V_p/V_s occur below the Central Ranges, except at shallow (<10 km) depths. The low seismicity under the Backbone Range Belt can be attributed to the high thermal gradient [*Wu et al.*, 1997] or simply that material in this region is ductile. Another consideration for low seismicity is the intrusion of fluid [*Chen and Chen*, 1998], but this viewpoint may not agree with the low V_p/V_s result.
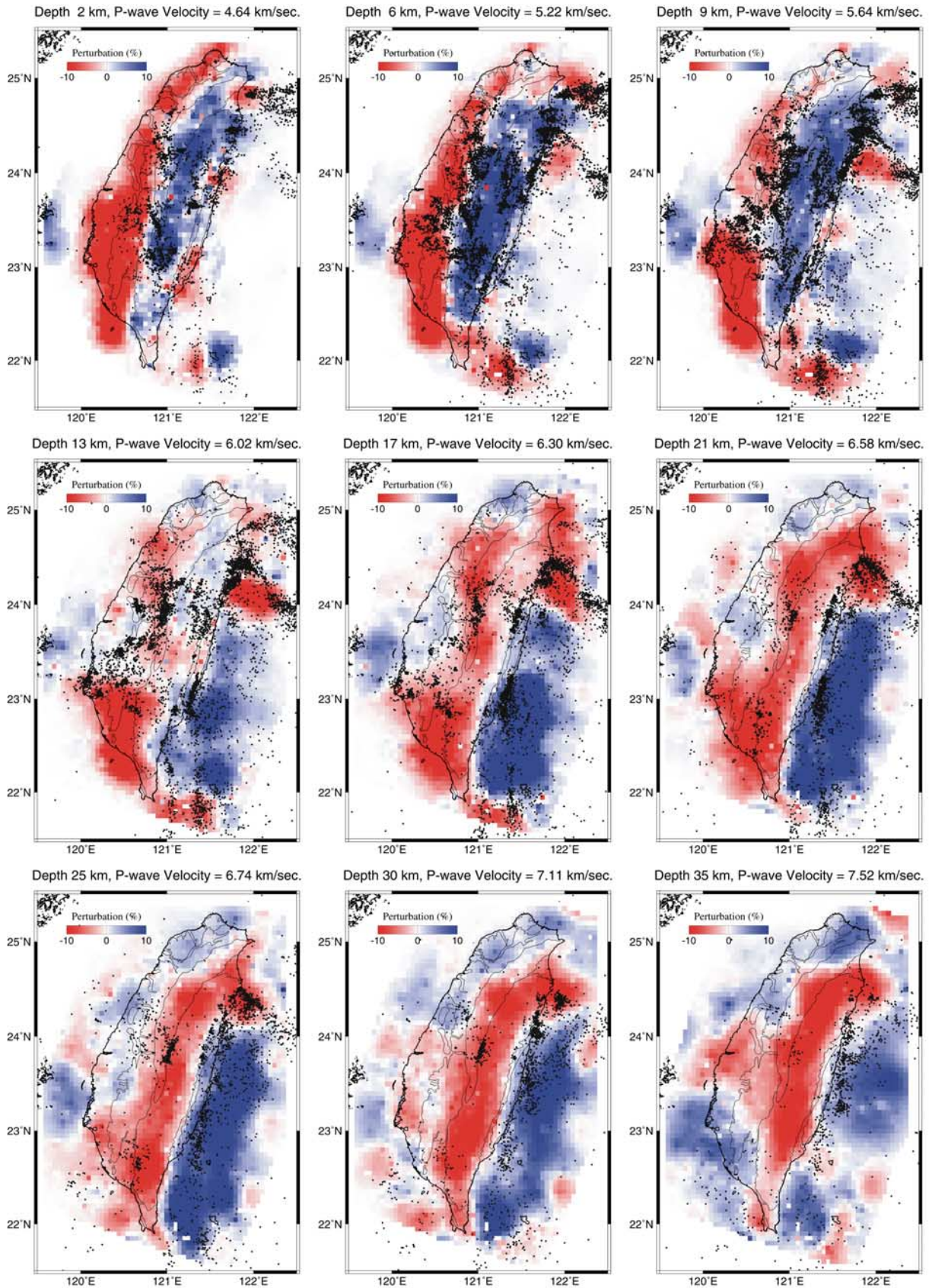
Figure 5a. V_p perturbation maps at nine different depths. Blue and red show high and low velocity, respectively. The dots show the relocated events for M > 3 within ±3 km of each layer. The depth and the reference P wave velocity are given for each plot.
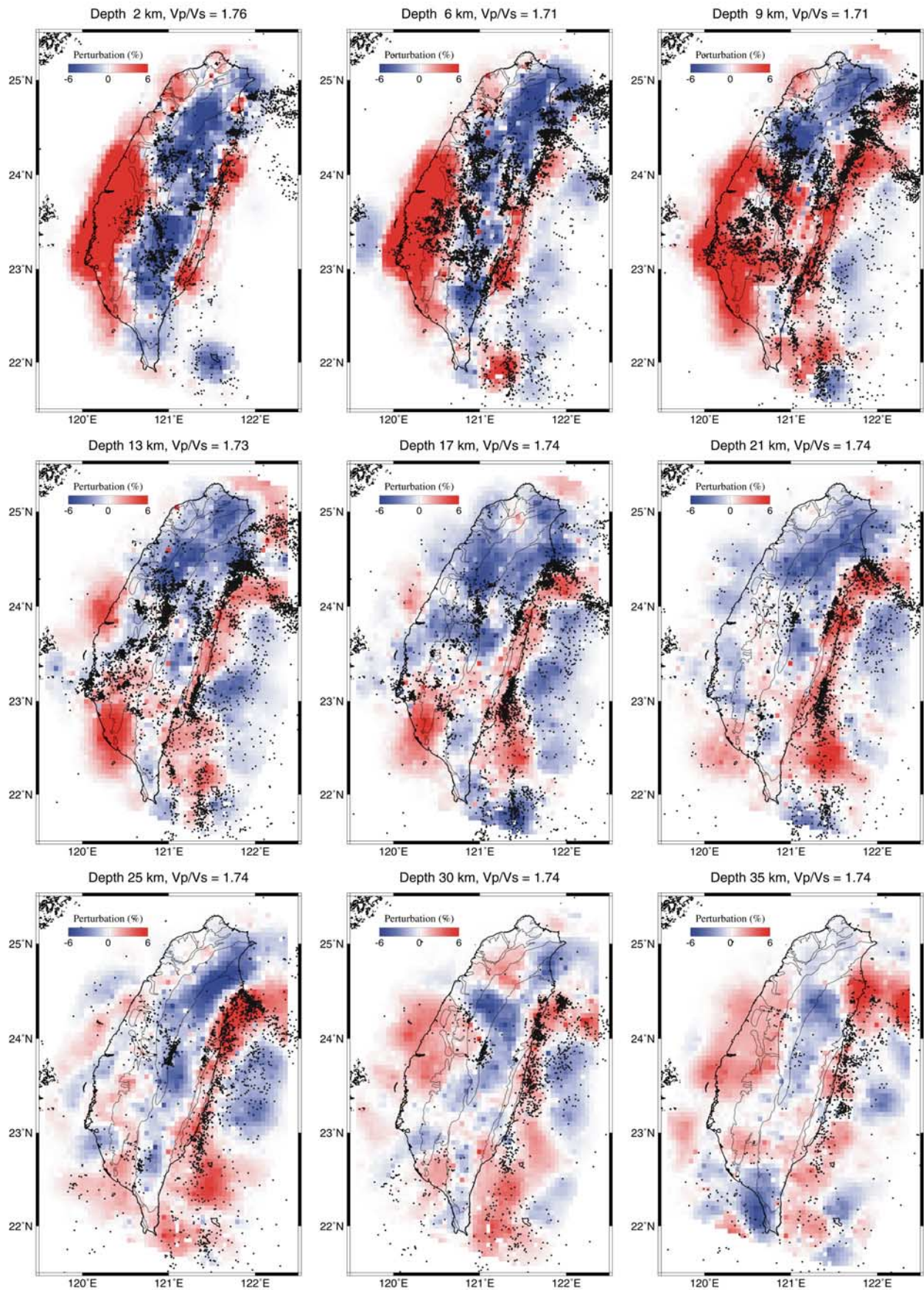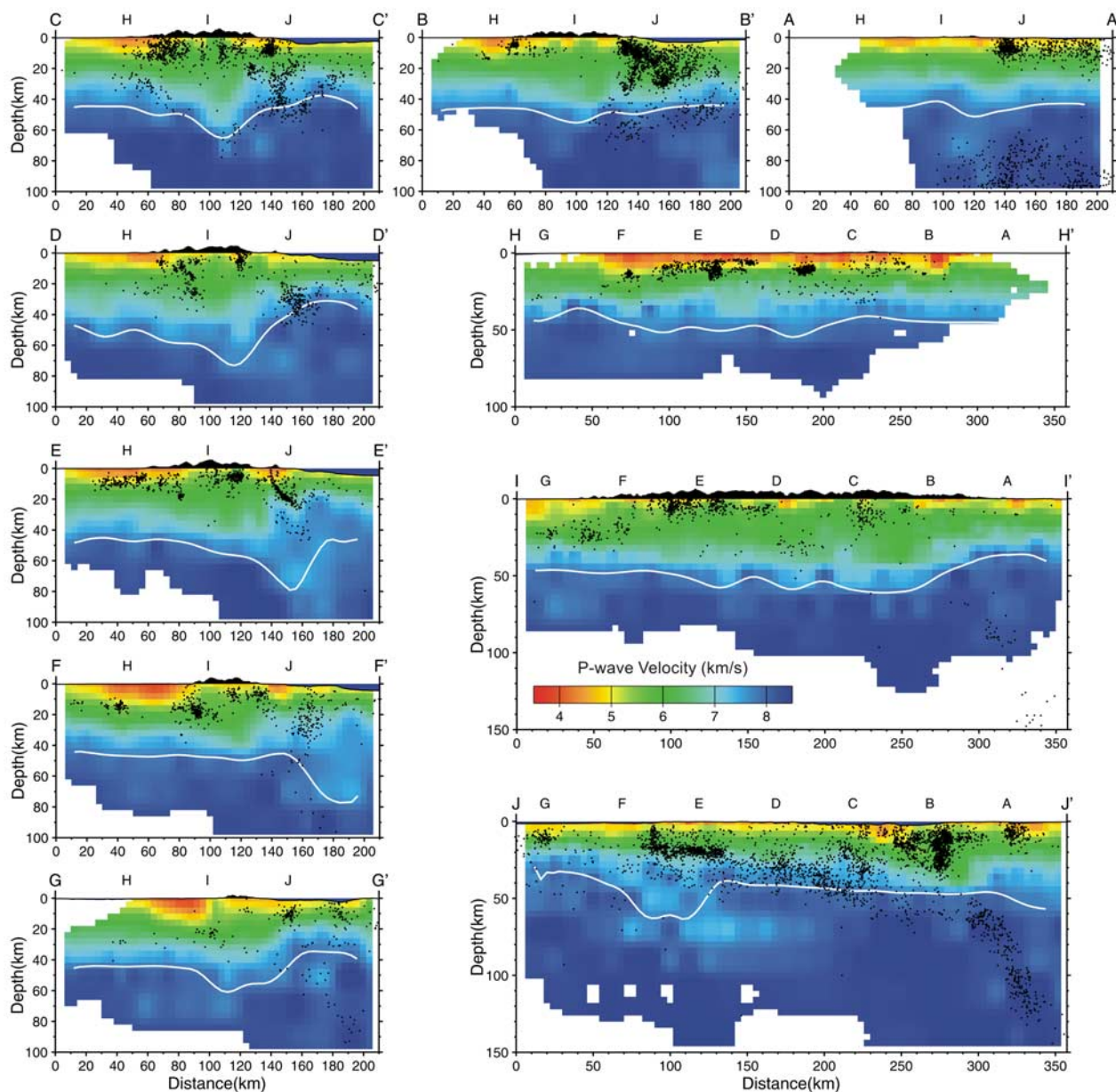
Figure 5b

Figure 6a. V_p velocity profiles. The dots show the relocated events for M > 3 within ±5 km of each profile. The white line shows V_p = 7.8 km/s for reference. Locations of the profiles A-A′ to J-J′ are indicated in Figure 2.

[24] The suture between the Central Ranges belt and the Luzon volcanic arc is characterized by a high V_p/V_s belt. The high V_p/V_s anomaly is generally coincident with zones of high seismicity, and in profile E-E′ in Figure 6b, the narrow high V_p/V_s anomaly is almost exactly colocated with the listric Longitudinal Valley fault plane illuminated by earthquakes. In profile B-B′ in Figure 6b, the high V_p/V_s anomaly extends deeper and appears to plunge to the west. We suspect that this pattern reflects the overriding of the middle to lower crust of the collided Luzon volcanic arc and the westernmost Philippine Sea plate by the northeastern part of the Central Ranges belt. As the suturing process that produced the island of Taiwan gives way to the northward subduction of the Philippine Sea plate along the Ryukyu trench, the northeastern Central Ranges belt has moved southeastward and has split apart from the Eurasian continental margin to form the Lanyang Plain which is geologically the southwestern extension of the Okinawa Trough

Figure 5b. V_p/V_s perturbation maps at the same nine depths as in Figure 5a. Red and blue show high and low V_p/V_s values, respectively. The dots show the relocated events for M > 3 within ±3 km of each layer. The depth and the reference V_p/V_s value are given for each plot.
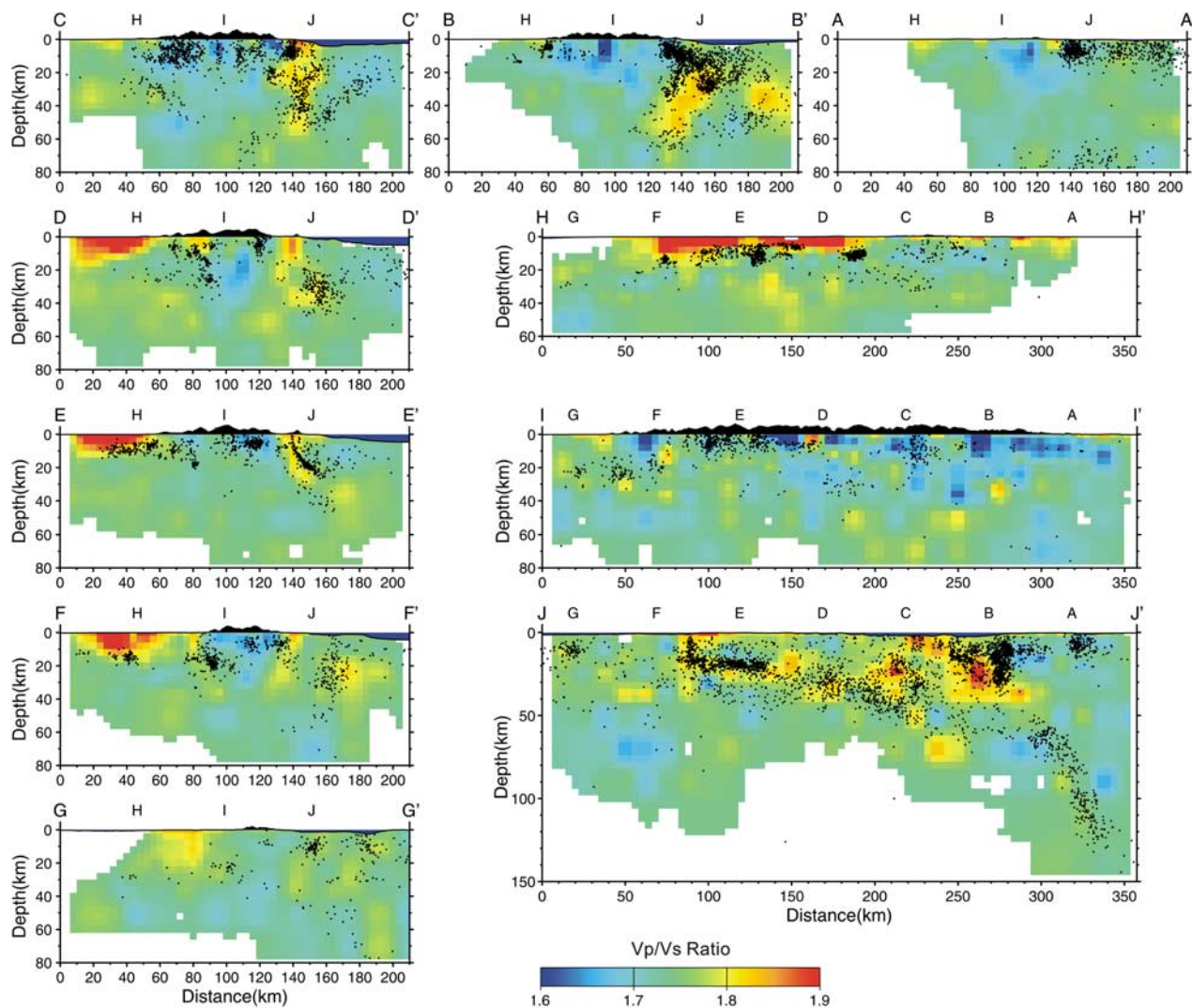
Figure 6b. V_p/V_s ratio profiles. The dots show the relocated events for M > 3 within ±5 km of each profile. Locations of the profiles A-A′ to J-J′ are indicated in Figure 2.

[e.g., *Shyu et al.*, 2005a, 2005b]. We believe that this has caused the northeastern Central Ranges belt to override the middle to lower crust of the collided Luzon volcanic arc. Westward bending and possible underthrusting of the western-most Philippine Sea plate is also observed from relocated seismicity in eastern Taiwan [*Kuochen et al.*, 2004].

5. Relocation of Seismicity

[25] We have used the new 3-D model obtained in this study to relocate a total of 35,530 events of M > 3 from 1990 to 2006. Figures 7a and 7b show the traveltime residuals before and after the relocation, respectively. Yellow 3 and blue dots show readings of high and low weightings, respectively. A total of 455,272 *P* wave arrival times, 178,382 *S* wave arrival times from the CWBSN, and 49,693 *S-P* times from the TSMIP stations are compiled here. For the CWBSN locations using 1-D model, the traveltime residuals have the means and standard deviations of 0.043 ± 0.500, −0.119 ± 0.631, and 0.023 ± 0.479 s for *P*, *S*, and *S-P* data, respectively. Figure 7a clearly shows that

the traveltime residuals for 1-D locations do not have a zero mean. In particular, *P* wave residuals tend to be slightly positive in the epicentral distance range from 150 to 250 km. *S* wave residuals are biased toward negative in the epicen-tral distance range from 30 to 100 km and positive from 110 to 280 km. *S-P* residuals are mostly negative in the epicentral distance range from 80 to 130 km. After the relocation using our 3-D model, the traveltime residuals have the means and standard deviations of −0.000 ± 0.358, −0.001 ± 0.536, and 0.012 ± 0.277 s for *P*, *S*, and *S-P* data, respectively. In particular, the standard deviation of the *S-P* residuals decreased by about 0.2 s, a 42% drop, since most of the *S-P* times was used in velocity inversion. Figure 7b clearly shows that the traveltime residuals after the 3-D relocation concentrate closely at zero especially for higher weighting samples (yellow dots). Also, the systematic shifts with distance have been removed.

[26] *Carena et al.* [2002] proposed an active detachment of Taiwan. The detachment subsurface at about 10-km depth runs from western Taiwan continuously to eastern Taiwan shown by the seismicity. In our relocated hypocenter
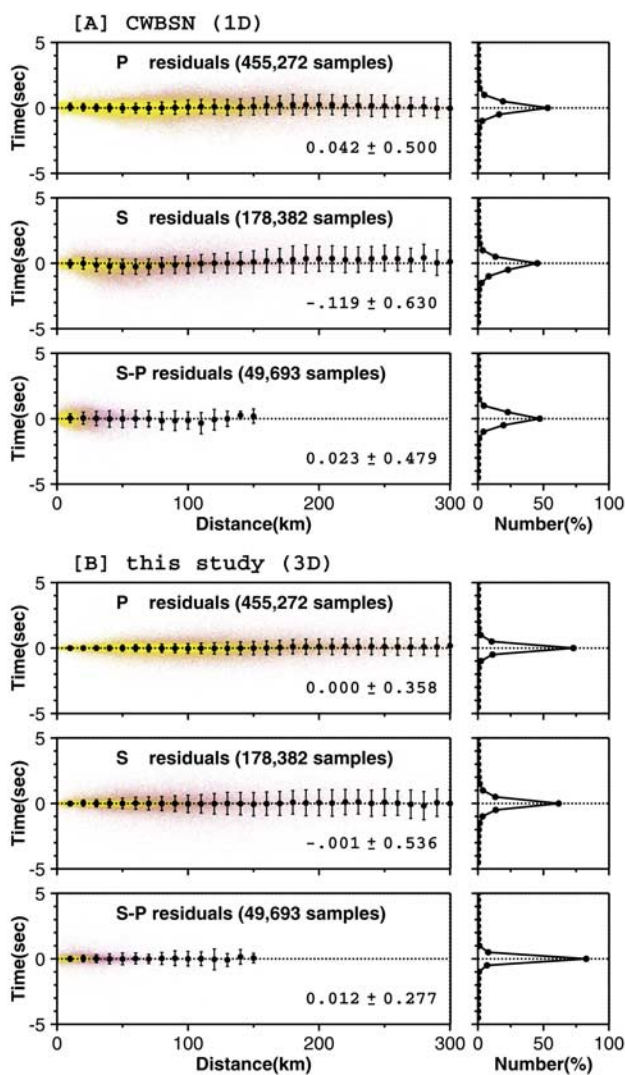
Figure 7. Residuals versus epicentral distances for the *P*, *S*, and S-*P* times predicted by the CWBSN locations using 1-D model and our locations using the 3-D model from this study.

distribution in Figures 5a and 5b, there is no continuous seismicity from western to eastern Taiwan. However, our data set only selected the events of M > 3.0 whereas *Carena et al.* [2002] used the events of M > 1.0. We suggest that small events may play an important role in such study. The V_p/V_s plot at depth 9 km (Figure 5b), the Chi-Chi earthquake source region and beneath the Central Ranges shows a high V_p/V_s pattern. It may be a signal of detachment to support the *Carena et al.* [2002]. However, this issue may warrant further investigation.

6. Discussion

[27] The only previous tomography study in the Taiwan region that presented both V_p and V_s models was that of *Kim et al.* [2005]. In that study, 6285 events from Taiwan Island

and the surrounding region were used to obtain 88,260 *P* and 63,522 *S* arrival times. Our model for the V_p structure is largely similar to that of *Kim et al.* [2005]. In addition, *Kim et al.* [2005] has a better resolution in the Hualien and Pingtung regions because of the two local dense networks they used in their tomography inversions. On the other hand, the events in this study are located in a larger region, and we used 3 times as many traveltime data. We also have a better constraint on the $V_{/p}V_s$ structure due to (1) the incorporation of the island-wide dense distribution of the 680 TSMIP stations from which we derived the *S-P* times, and (2) the inversion of the V_p/V_s model directly from the *S-P* times, which effectively eliminates the possible errors in earthquake origin times.

[28] Figure 8 shows V_p velocity and V_p/V_s ratio profiles in eastern Taiwan with the same location of profile FF' in Figure 13 of *Kim et al.* [2005], the dots show the relocated events for M > 3 within a 5-km zone on either side of each profile. The location of the profile is indicated by e-e' in
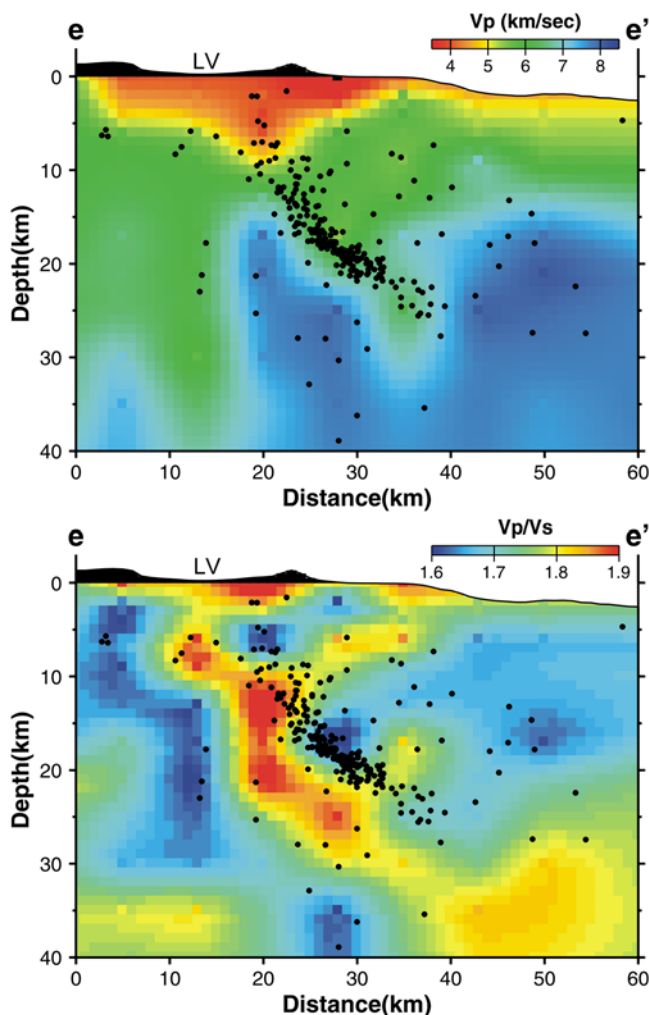

Figure 8. V_p velocity and V_p/V_s ratio profiles in eastern Taiwan. The dots show the relocated events for M > 3 within ±5 km of each profile. Location for the e-e' profile is shown in Figure 2. LV marks the location of Longitudinal Valley.

Figure 2. In comparison with *Kim et al.* [2005] the V_p patterns are similar with a large velocity contrast across the Longitudinal Valley. However, the results are very different in V_p/V_s ratio and the relocated seismicity. The events used are different but the seismicity pattern is similar. *Kim et al.* [2005] related the high seismicity to high V_p/V_s. In our result, however, the relocated seismicity concentrates above the curved zone dipping to the east delineated by the high V_p/V_s pattern. The relocated hypocenters are not situated on the high V_p/V_s as by *Kim et al.* [2005]. In contrast, they are located in between high and low V_p/V_s zones. We suggest that the high V_pV_s correlates to the suture zone and the seismicity above is related to the Coastal Ranges fault as propose in our previous study [*Wu et al.*, 2006a]. In profile F-F′ in Figure 6b, the high V_p/V_s zone in the Taitung region dips to the west with high angle. This pattern is consistent with our recent observation [*Wu et al.*, 2006b] that in the Taitung region there may be a boundary fault dipping to the west with a high angle in association with the Central Ranges fault. This fault is recently proposed as another major active structure along the Longitudinal Valley suture on the basis of geomorphic observations [*Shyu et al.*, 2006].

7. Conclusions

[29]   In this study, we combined a large data set of *S-P* times from the TSMIP records with the *P* and *S* wave arrival times from the CWBSN network in imaging the regional 3-D *P* wave and V_p/V_s structures in Taiwan. The TSMIP data set improves the source-station path coverage tremendously and provides much better constraints and resolution in velocity structure determination. The new 3-D V_p and V_p/V_s structures and the relocated seismicity provide several new insights for Taiwan's regional seismotectonics. The plate boundary can be identified clearly by the V_p structures. As seen in Figure 5a, V_p structure is clearly divided into three high-low-high zones from west to east at the depth of 25 km. The western high-V_p zone represents the foreland of the Eurasian plate. The middle low-V_p zone under the Central Ranges represents the basement of the Central Ranges belt, which has high V_p at shallow depths and low V_p at greater depths. This is typical of mountain roots. The V_p profiles in Figure 6a show that the Moho interface may reach down to 60-km depth under the Central Ranges. The eastern high-V_p structures clearly show the western boundary of the Philippine Sea Plate, with the Longitudinal Valley as the suture zone. On the eastern side of the Longitudinal Valley are zones of high V_p and V_p/V_s structures with a high seismicity. They represent the island arc collision zone. The high V_p/V_s may indicate a fracture zone and may reflect the existence of fluids. This zone subducts under the Eurasian Plate in the N20°E direction and also plunges to the west under the Central Ranges from Hualien to Ilan region.

References

Carena, S., J. Suppe, and H. Kao (2002), Active detachment of Taiwan illuminated by small earthquakes and its control of first-order topography, *Geology*, 30, 935–938.

Chen, C. C., and C. S. Chen (1998), Preliminary result of magnetotelluric soundings in the fold-thrust belt of Taiwan and possible detection of dehydration, *Tectonophysics*, 292, 101–117.

Chen, K.-C. (1995), Earthquake studies using the PANDA and PANDAII seismic array, Ph.D. thesis, CERI/Dep. of Geol. Sci., Univ. of Memphis, Memphis, Tenn.

Chen, K.-P. (1998), Study of shallow structure beneath Kaoshiung–Pingtung region using local earthquake data, Ph.D. thesis, Inst. of Geophys., Natl. Central Univ., Jungli, Taiwan.

Eberhart-Phillips, D. (1986), Three-dimensional *P* and *S* velocity structure in northern California Coast ranges from inversion of local earthquake arrival times, *Bull. Seismol. Soc. Am.*, 76, 1025–1052.

Eberhart-Phillips, D. (1990), Three-dimensional *P* and *S* velocity structure in the Coalinga region, California, *J. Geophys. Res.*, 95, 15,343–15,363.

Eberhart-Phillips, D. (1993), Local earthquake tomography: Earthquake source regions, in *Seismic Tomography: Theory and Practice*, edited by H. M. Iyer and K. Hirahara, pp. 613–643, Chapman and Hall, New York.

Evans, J. R., D. Eberhart-Philips, and C. H. Thurber (1994), User's manual for SIMULPS12 for imaging V_p and V_p/V_s: A derivative of the "Thurber" tomography inversion SIMUL3 for local earthquakes and explosions, *U.S. Geol. Surv. Open File Rep., 94-431*, 100 pp.

Ho, C. S. (1999), *An Introduction to the Geology of Taiwan. Explanatory Text of the Geologic Map of Taiwan*, Central Geol. Surv., Minist. of Econ. Affairs, Taipei, Taiwan.

Hole, J. A., T. M. Brocher, S. L. Klemperer, T. E. Parsons, H. M. Benz, and K. P. Furlong (2000), Three-dimensional seismic velocity structure of the San Francisco Bay area, *J. Geophys. Res.*, 105, 13,859–13,874.

Huang, C. Y., C. T. Shyu, S. B. Lin, T. Q. Lee, and D. D. Sheu (1992), Marine geology in the arc-continent collision zone off southeastern Taiwan: Implications for Late Neogene evolution of the Coastal Range, *Mar. Geol.*, 107, 183–212.

Kao, H., G.-C. Huang, and C.-S. Liu (2000), Transition from oblique subduction to collision in the northern Luzon arc-Taiwan region: Constraints from bathymetry and seismic observations, *J. Geophys. Res.*, 105, 3059–3079.

Kim, K. H., J. M. Chiu, J. Pujol, K. C. Chen, B. S. Huang, Y. H. Yeh, and P. Shen (2005), Three-dimensional V_p and V_s structural model associated with the active subduction and collision tectonics in the Taiwan region, *Geophys. J. Int.*, 162, 204–220.

Kissling, E., W. L. Ellsworth, D. Eberhart-Phillips, and U. Kradolfer (1994), Initial reference models in local earthquake tomography, *J. Geophys. Res.*, 99, 19,635–19,646.

Kuochen, H., Y. M. Wu, C. H. Chang, J. C. Hu, and W. S. Chen (2004), Relocation of the eastern Taiwan earthquakes and its tectonic implications, *Terr. Atmos. Oceanic Sci.*, 15, 647–666.

Lee, W. H. K., and J. C. Lahr (1975), HYPO71 (revised): A computer program for determining hypocenter, magnitude and first motion pattern of local earthquakes, *U.S. Geol. Surv. Open File Rep., 75-311*.

Ma, K. F., J. H. Wang, and D. Zhao (1996), Three-dimensional seismic velocity structure of the crust and uppermost mantle beneath Taiwan, *J. Phys. Earth*, 44, 85–105.

Mouthereau, F., B. Deffontaines, O. Lacombe, and J. Angelier (2002), Variations along the strike of the Taiwan thrust belt: Basement control on structural style, wedge geometry, and kinematics, in *Geology and Geophysics of an Arc-Continent Collision*, edited by T. B. Byrne and C.-S. Liu, *Spec. Pap. Geol. Soc. Am.*, 358, 31–54.

Pavlis, G. L., and J. R. Booker (1980), The mixed discrete-continuous inverse problem: Application to the simultaneous determination of earthquake hypocenters and velocity structure, *J. Geophys. Res.*, 85, 4801–4810.

Rau, R.-J., and F. T. Wu (1995), Tomographic imaging of lithospheric structures under Taiwan, *Earth Planet. Sci. Lett.*, 133, 517–532.

Roecker, S. W., Y. H. Yeh, and Y. B. Tsai (1987), Three-dimensional *P* and *S* wave velocity structures beneath Taiwan; deep structure beneath an arc-continent collision, *J. Geophys. Res.*, 92, 10,547–10,570.

Shin, T. C., and Y. L. Chen (1988), Study on the earthquake location of 3-D velocity structure in the Taiwan area, *Meteorol. Bull.*, 42, 135–169.

Shin, T. C., Y. B. Tsai, Y. T. Yeh, C. C. Liu, and Y. M. Wu (2003), Strong-motion instrumentation programs in Taiwan, in *Handbook of Earthquake and Engineering Seismology*, edited by W. H. K. Lee et al., pp.1057–1062, Academic, San Diego, Calif.

Shyu, J. B. H., K. Sieh, Y.-G. Chen, and C.-S. Liu (2005a), Neotectonic architecture of Taiwan and its implications for future large earthquakes, *J. Geophys. Res.*, 110, B08402, doi:10.1029/2004JB003251.

Shyu, J. B. H., K. Sieh, and Y. G. Chen (2005b), Tandem suturing and disarticulation of the Taiwan orogen revealed by its neotectonic elements, *Earth Planet. Sci. Lett.*, *233*, 167–177.

Shyu, J. B. H., K. Sieh, Y. G. Chen, and L. H. Chung (2006), Geomorphic analysis of the Central Range fault, the second major active structure of the Longitudinal Valley suture, eastern Taiwan, *Geol. Soc. Am. Bull.*, *118*, 1447–1462.

Suppe, J. (1984), Kinematics of arc-continent collision, flipping of subduction, and back-arc spreading near Taiwan, *Mem. Geol. Soc. China*, *6*, 21–33.

Thurber, C. H. (1983), Earthquake locations and three-dimensional crustal structure in the Coyote Lake area, central California, *J. Geophys. Res.*, *88*, 8226–8236.

Thurber, C. H. (1993), Local earthquake tomography: Velocities and V_p/V_s—Theory, in *Seismic Tomography: Theory and Practice*, edited by H. M. Iyer and K. Hirahara, pp. 563–583, Chapman and Hall, London.

Thurber, C., and D. Eberhart-Phillips (1999), Local earthquake tomography with flexible gridding, *Comput. Geosci.*, *25*, 809–818.

Um, J., and C. H. Thurber (1987), A fast algorithm for two-point seismic ray tracing, *Bull. Seism. Soc. Am.*, *77*, 972–986.

Wang, Z., D. Zhao, J. Wang, and H. Kao (2006), Tomographic evidence for the Eurasian lithosphere subducting beneath south Taiwan, *Geophys. Res. Lett.*, *33*, L18306, doi:10.1029/2006GL027166.

Wu, F. T., R. J. Rau, and D. Salzberg (1997), Taiwan orogeny: Thin-skinned or lithospheric collision?, *Tectonophysics*, *274*, 191–220.

Wu, Y. M., Y. G. Chen, T. C. Shin, H. Kuochen, C. S. Hou, J. C. Hu, C. H. Chang, C. F. Wu, and T. L. Teng (2006a), Coseismic versus interseismic ground deformations, fault rupture inversion and segmentation revealed by 2003 *Mw* 6.8 Chengkung earthquake in eastern Taiwan, *Geophys. Res. Lett.*, *33*, L02312, doi:10.1029/2005GL024711.

Wu, Y.-M., Y.-G. Chen, C.-H. Chang, L.-H. Chung, T.-L. Teng, F. T. Wu, and C.-F. Wu (2006b), Seismogenic structure in a tectonic suture zone: With new constraints from 2006 *Mw* 6.1 Taitung earthquake, *Geophys. Res. Lett.*, *33*, L22305, doi:10.1029/2006GL027572.

Yeh, Y. H., R. C. Shih, C. H. Lin, C. C. Liu, H. Y. Yen, B. S. Huang, C. S. Liu, and F. T. Wu (1998), Onshore/offshore wide-angle deep seismic profiling in Taiwan, *Terr. Atmos. Oceans*, *9*, 301–316.

Yu, S. B., H. Y. Chen, L. C. Kuo, S. E. Lallemand, and H. H. Tsien (1997), Velocity field of GPS stations in the Taiwan area, *Tectonophysics*, *274*, 41–59.

Zhao, D., A. Hasegawa, and S. Horiuchi (1992), Tomographic imaging of *P* and *S* wave velocity structure beneath northeastern Japan, *J. Geophys. Res.*, *97*, 19,909–19,928.

————————————

J.-P. Avouac, J. B. H. Shyu, and K. Sieh, Tectonics Observatory, California Institute of Technology, Pasadena, CA 91125, USA.

C.-H. Chang, Central Weather Bureau, 64 Kung Yuan Road, Taipei, Taiwan.

Y.-G. Chen and Y.-M. Wu, No. 1, Sec. 4th, Roosevelt Road, Department of Geosciences, National Taiwan University, Taipei, Taiwan. (drymwu@ntu.edu.tw)

L. Zhao, Institute of Earth Sciences, Academia Sinica, Nankang, Taipei 115, Taiwan.